PHOTOMETRIC EVOLUTION OF THE DEEP IMPACT FLASH. C. M. Ernst, P. H. Schultz, M. F. A'Hearn and the Deep Impact Science Team, Brown University, Department of Geological Sciences, Box 1846, Providence, RI 02912 (Carolyn_Ernst@brown.edu).

Introduction: On July 4, 2005, the Deep Impact (DI) mission performed a planetary-scale impact experiment into comet 9P/Tempel 1. A 360 kg impactor transported 19 GJ of kinetic energy to the nucleus at a velocity of 10.2 km/s, producing a prolonged radiant impact flash observed by the DI flyby spacecraft. The mission has provided a crucial planetary-scale data point that can be compared to data from laboratory-scale experiments.

Observations: The impact with Tempel 1 occurred at an angle of 20º-40º from the horizontal [1]. The Medium Resolution Imager (MRI) on board the flyby spacecraft recorded an image sequence around the time of impact with a time resolution of 62 ms (51.5 ms exposure plus readout time) at a very oblique view angle. Figure 1 shows the first ~500 ms after impact, taken through a clear filter (0.32-1.05 μm). The initial flash or "first light" was relatively small and dim (frame A). All times referenced here are relative to the time after the first light image. A delayed second flash began after ~124 ms (C) and quickly brightened to the point of saturation (D), leading to charge bleeding. As the bright flash evolved further, a plume expanded downrange away from the point of impact (E-G). By 310 ms (F) the central light signal remaining around the point of impact consisted of reflected light from the expanding ejecta plume. Figure 2 reveals that the flash (A-D) appears to move along the initial impactor trajectory.

Interpretation: The faint flash followed by the delayed saturated flash farther downrange can be explained by an oblique impact into a low-density (0.3 g/cc) target as documented in laboratory experiments [2-4]. In this scenario, the first light is a plume of dust and gas directed uprange of the initial penetration funnel due to cavitation (implosion and redirection of vapor). In laboratory experiments, this initial plume is highly collimated [e.g., 5] and is faint due to the low affected mass (due to an extremely high target porosity) [3] and/or the dominance of vapor phases (little thermal radiation) [6].

As the initial penetration funnel opens, shock-heated vapor emerges downrange and retains a substantial fraction of the initial impact velocity [3]. Vapor expansion adds an additional component to the leading edge. Tracing the downrange plume back to the moment of emergence from the surface indicates that this component should appear ~100 ms after first light. The subsequent delay in the bright flash can be interpreted as the combination of the time between the opening of the penetration funnel, obscuration during projectile entry, and the initial dearth of thermal radiation (dominance of emission lines).

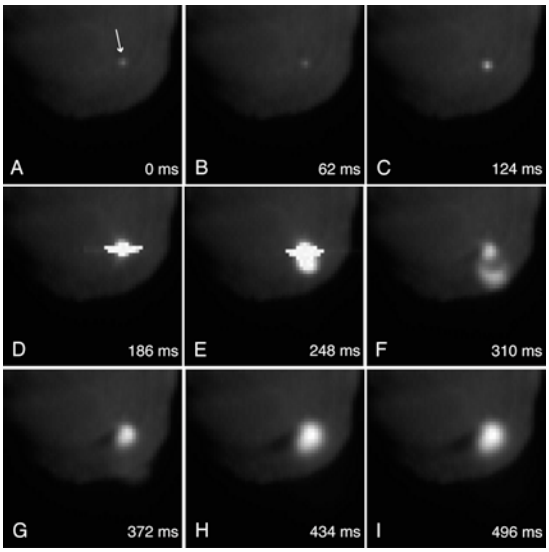

Figure 1. The first nine frames (~500 ms) after impact from the MRI. The initial dim "first light" signal was overtaken by a delayed bright (saturated) signal after 186 ms. The vapor plume can be seen expanding downrange away from the site of impact beginning in frame E. The arrow indicates the direction of impact.

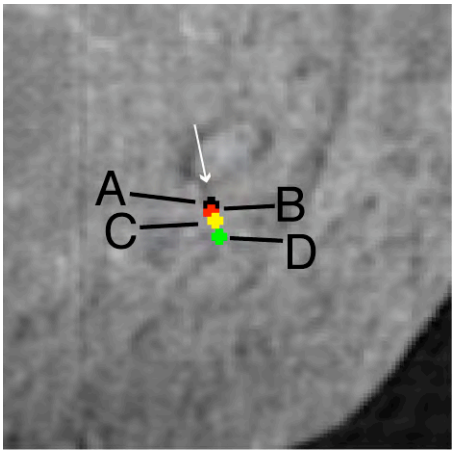

Figure 2. The migration of the impact flash. The letters correspond to the frame letters from Figure 1: A represents the location of the first light, C the beginning of the delayed second flash (100-200 m downrange), and D the center of brightness of the first saturated image, likely due to the emergence of the hot vapor/gas. The background image is a subset of the comet surface observed before impact.

Experimental oblique impacts produce a downrange-moving vapor plume traveling along the surface at a velocity comparable to the initial impact

velocity while expanding hemispherically [2,5]. On a three-dimensional body, this plume evolves into a spherically expanding cloud. The oblique view angle of the DI collision requires that the downrange plume velocity be corrected for the projection. Consequently, the observed downrange speed of ~6 km/s for the leading edge becomes 8-12 km/s (depending on the projection angle). The lateral expansion speed of the leading edge of the self-luminous downrange plume is about 2.3 km/s and is related to the total internal energy of the vapor fraction.

If it is assumed that H_2O and CO_2 vapor primarily control gas expansion, then the observed lateral expansion (2.3 km/s) for the DI downrange plume is consistent with extrapolations from laboratory experiments for oblique impacts into dry-ice (2.7 km/s) and water-ice (2.4 km/s) targets [5]. This result provides an estimate for the internal energy of the vapor cloud (~30% initial energy) and total vaporization (vapor/projectile mass ≈6 for H_2O and ≈30 for CO_2) in the downrange expanding plume.

Intensity Analysis: The evolution of the DI light intensity is shown in Figure 3. The intensity of the entire central reflected-light portion of the signal initially underwent linear growth (beginning in frame F), but after 682 ms its growth began to slow, diverging from the linear trend. The self-luminous impact flash is of primary interest here; the reflected light was not part of the flash. The self-luminous component includes the light flux integrated over not only the early central light flash (A-F) but also the expanding downrange plume. The primary light source is thermal radiation from heated and melted ejecta particulates.

The luminous efficiency (in the visible wavelength range) of the DI flash was predicted to be ~$8x10^{-4}$ based on experiments into non-volatile pumice dust targets [2]. The measured luminous efficiency observed by the MRI was ~10^{-8}. This large difference is due to the use of a pumice dust-like target for laboratory experiments. Nevertheless, the flash duration was comparable to expectations [2].

Experimental impacts were performed at the NASA Ames Vertical Gun Range to explore the effect of target porosity and volatile content on the resulting impact flash. The experiments showed that the more porous a target surface, the lower the luminous efficiency of the impact. This is a result of the deeper penetration of the projectile into the more porous target and the less mass encountered.

Volatiles in the target surface also decrease the luminous efficiency of the impact. Some of the transferred kinetic energy is partitioned into vaporization and vapor expansion, and much of the emitted light is in the form of emission lines as opposed to a blackbody continuum [7]. Figure 4 illustrates the difference in the light evolution for impacts into targets of different porosity and volatile content.

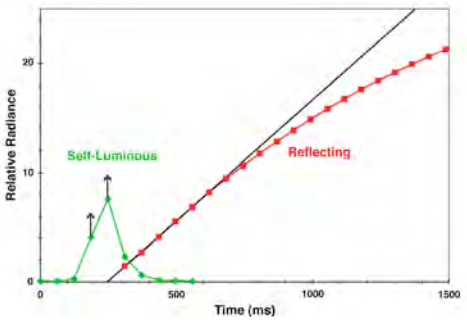

Figure 3. Intensity evolution of the Deep Impact collision. The green curve represents the self-luminous portion of the light output and is considered to be the "flash", while the red curve represents light reflected off of the emerging ejecta. The black line is the initial linear growth trend of the reflecting portion extrapolated through time. The intensity values for the saturated images represent minimum values.

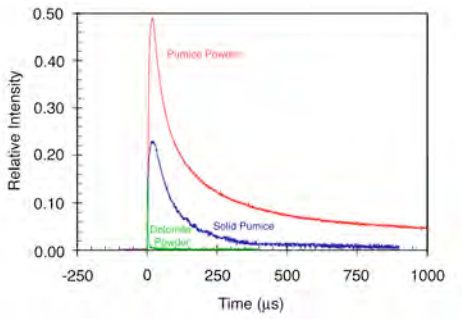

Figure 4. The intensity evolution of experimental impacts into targets of different porosity and volatile content. Both greater porosity (seen in the difference between the pumice powder and solid pumice targets) and greater volatile content (seen in the difference between the pumice powder and the dolomite powder targets) lead to a suppression of the luminous output.

Conclusions: The DI collision produced a complex light flash that evolved in brightness and location over time. The movement can be explained by the creation of both the uprange and the downrange plumes, as well as possible obscuration during the early stages after impact. The overall luminous efficiency of the flash was far lower than predicted, most likely due to the high porosity and volatile content of the Tempel 1 surface.

Acknowledgements: This research is supported by NASA through the Discovery Program's *Deep Impact* mission.

References: [1] A'Hearn, M. F. et al. (2005) *Science, 310*, 258-264. [2] Schultz, P. H. et al. (2005) *SSR, 117*, 207-239. [3] Ernst, C. M. and P. H. Schultz (2003) *LPS XXXIV*, #2020. [4] Schultz, P. H. and J. L. B. Anderson (2005) *LPS XXXVI*, #1926. [5] Schultz, P. H. (1996) *JGR, 101*, 21,117-21,136. [6] Ernst, C. M. and P. H. Schultz (2005) *LPS XXXVI*, #1475. [7] Eberhardy, C. A. and P. H. Schultz (2004) *LPS XXXV*, #1855.